Geofísica Internacional (2026) **65-3**: 2339- 2355

Tropospheric Correction using PyAPS in the West Region of Venezuela

Gabriela Quintana Sánchez[1,*,a], Carlos Reinoza[2,b], Fikret Dogru[3,c], Gareth Funning[4,d] and Franck Audemard[5,e]

Abstract

The subsidence of the East Coast of Lake Maracaibo-COLM in Zulia state in Venezuela is a geological event of anthropic cause with almost a century of existence. We wanted to know the current state of this event with the use of the Interferometric Synthetic Aperture Radar-InSAR technique, for this, we emphasized the need to mitigate atmospheric delays in the data, for which the ERA5 climate model with PyAPS was applied. In order to obtain accurate subsidence measurements in three oil fields located in the COLM (Tia Juana, Lagunillas and Bachaquero), whose cumulative subsidence process is approximately 5 meters between 1926 and 1986. For this study, subsidence values were estimated, for the period from 2018 to 2020, using a dataset of 157 interferometric Sentinel-1 images (79 from ascending orbits and 78 from descending orbits), which allowed the calculation of the values of displacements along the line of sight-LOS for both orbits, the tropospheric delay contribution, and the east-west and vertical components values, extracted from representative pixels with high coherence and with spatial and temporal average, having random noise component reduced, obtaining displacement values for Tia Juana, Lagunillas and Bachaquero fields respectively of: -6.4 +/- 0.8 cm/y; -7.9 +/- 1.0 cm/y and; -7.1 +/- 0.8 cm/y, for ascending mode. From 1.2 +/- 0.5 cm/y; -4.1 +/- 0.5 cm/y and; -1.8 +/- 0.3 cm/y, for descending mode. Also, by selecting representative pixels, we estimated reliable values for contribution from tropospheric delay, obtaining: -0.2 cm/y and -0.6 cm/y; -0.3 cm/y and -0.5 cm/y and; -0.4 cm/y and -0.5 cm/y. And the east-west (dE) and vertical (dU) components for the three fields, with: -6.79 cm/y and -2.94 cm/y; -3.27 cm/y and -5.19 cm/y and; -5.92 cm/y and -6.29 cm/y respectively, minimizing the risk that geometric projection errors will amplify underlying noise.

Key words: InSAR, Displacement, Subsidence, COLM, Venezuela.

Resumen

La subsidencia de la Costa Oriental del Lago de Maracaibo (COLM) en el estado Zulia, Venezuela, es un evento geológico de causa antrópica con casi un siglo de existencia. Se buscó conocer el estado actual de este evento mediante el uso de la técnica de Interferometría de Radar de Apertura Sintética (InSAR); para ello, se enfatizó la necesidad de mitigar los retrasos atmosféricos en los datos, por lo que se aplicó el modelo climático ERA5 con PyAPS. Esto con el fin de obtener mediciones precisas de la subsidencia en tres campos petroleros ubicados en la COLM (Tía Juana, Lagunillas y Bachaquero), cuyo proceso de subsidencia acumulada es de aproximadamente 5 metros entre 1926 y 1986. Para este estudio, se estimaron los valores de subsidencia para el período de 2018 a 2020 utilizando un conjunto de datos de 157 imágenes interferométricas de Sentinel-1 (79 de órbitas ascendentes y 78 de órbitas descendentes), lo que permitió calcular los valores de desplazamiento a lo largo de la línea de visión (LOS) para ambas órbitas, los valores de la contribución del retraso troposférico y los valores de las componentes este-oeste y vertical, extraídos de píxeles representativos con alta coherencia y con promedio espacial y temporal, habiendo reducido la componente de ruido aleatorio. Se obtuvieron valores de desplazamiento para los campos de Tía Juana, Lagunillas y Bachaquero, respectivamente, de: -6.4 +/- 0.8 cm/año, -7.9 +/- 1.0 cm/año y -7.1 +/- 0.8 cm/año para el modo ascendente; y de 1.2 +/- 0.5 cm/año, -4.1 +/- 0.5 cm/año y -1.8 +/- 0.3 cm/año para el modo descendente. Asimismo, mediante la selección de píxeles representativos, se estimaron valores confiables para la contribución del retraso troposférico, obteniendo: -0.2 cm/año y -0.6 cm/año; -0.3 cm/año y -0.5 cm/año y; -0.4 cm/año y -0.5 cm/año. Por último, las componentes este-oeste (dE) y vertical (dU) para los tres campos fueron de: -6.79 cm/año y -2.94 cm/año; -3.27 cm/año y -5.19 cm/año; y -5.92 cm/año y -6.29 cm/año, respectivamente, minimizando el riesgo de que los errores de proyección geométrica amplifiquen el ruido subyacente.

Palabras clave: InSAR, Desplazamiento, Subsidencia, COLM, Venezuela.

Received: October 29, 2025; Accepted: May 2, 2026; Published on-line: July 1, 2026. https://doi.org/10.22201/igeof.2954436xe.2026.65.3.1930

Editorial responsibility: Mtro. Miguel Moctezuma-Flores, Universidad Nacional Autónoma de México, Facultad de Ingeniería.

* Corresponding author: Gabriela Quintana, gabrielaquintana77@gmail.com

[1] Universidad Central de Venezuela (UCV), Facultad de Ingeniería. Escuela de Geología, Minas y Geofísica. Fundación Venezolana de Investigaciones Sismológicas (FUNVISIS), Venezuela.

[2] Centro de Investigación Científica y de Educación Superior de Ensenada (CICESE), Baja California, México.

[3] Ataturk University, Oltu Vocational College, Construction, Erzurum, Turquía.

[4] University of California Riverside, California, United States of America.

[5] Universidad Central de Venezuela (UCV), Facultad de Ingeniería. Escuela de Geología, Minas y Geofísica.

ORCID: [a]0009-0008-0128-7441, [b]000-0003-2347-3161, [c]0000-0002-6973-1157, [d]000-0002-8247-0545, [e]000-0003-2046-5916.

1. Introduction

The usefulness of Synthetic Aperture Radar images for Earth observation began in the 1950s for military purposes. Its expansion into the geoscientific world began with the launch of the SEASAT civilian satellite in 1978 and with other subsequent missions (Meng *et al.*, 2024).

Geoscientists around the world have applied the Interferometric Synthetic Aperture Radar-InSAR technique in the study of crustal deformations. This tool has made it possible to improve the detection, quantification and characterization of processes, both natural, such as: aquifer dynamics, tectonic and magmatic processes, etc.; (Biggs & Wright, 2020; González, 2024; Medici *et al.* 2024; Meng *et al.* 2024) as those induced by human activities that cause movements of the surface.

One of the human activities that induces surface deformation refers to the extraction of fluids, such as: hydrocarbons and groundwater, added to constructed buildings and infrastructure on top can generate deformation and collapse of the ground. Also, the process of compactation and rearrangement of the sediments, alongside a significant reduction of pore space within subsurface layers have high contribution to the loss of surface elevation (Poland and Davis, 1969). In this context, the Interferometry Synthetic Aperture Radar-InSAR has transformed our understanding of Earth dynamics by imaging the entire Earth's surface. With the launch of the Sentinel-1 pairs, in 2014, a reliable and long-term archive of ground-based InSAR measurements is available, to support the monitoring and mitigation of soil movements from anthropogenic and/or natural sources, affecting the civil, geotechnical and structural engineering sectors (Biggs and Wright, 2020).

However, a limitation in the use of satellite radar data for the detection of crustal deformations lies in atmospheric signals (Agram *et al.*, 2013, Dogru *et al.*, 2023), which often mask actual displacement, particularly in mountainous areas (Brencher *et al.*, 2023; Dogru *et al.*, 2023).

According to Hu and Mallorquí (2019), phase noise in InSAR is classified into two types according to its origin. The first is of ionospheric origin, occurring in spectral bands such as P or L due to fluctuations in electron density between 100 and 1000 km altitude, which alters the signal path (Gray *et al.*, 2000). The second type is tropospheric delays, caused by variations in temperature, pressure, and humidity (Chen *et al.*, 2025). These delays combine a turbulent component (affecting flat and mountainous terrain, with high spatial correlation but low temporal correlation) and a stratified component (directly correlated with topography, which only distorts measurements in areas with unevenness such as hills or mountains) (Hanssen, 2001; Xiao *et al.*, 2021). The total delay is calculated according to Equation 1 by integrating the differential hydrostatic (temperature and pressure) and differential wet (water vapor) components between the surface and the satellite elevation along the line of sight (LOS) (Equation 1, Hanssen, 2001):

$$\Delta\delta L_{\mathrm{atm}}^{InSAR} = \frac{10^{-6}}{\cos\theta}\left[\frac{k_1 R_d}{g_m}\Delta P_{\mathrm{diff}} + \int_{Z_{\mathrm{surf}}}^{Z_{\mathrm{top}}}\left(k_2'\frac{\Delta_e}{T}k_3\frac{\Delta_e}{T^2}\right)dz\right] \tag{1}$$

Where: θ = incident angle. $\Delta P_{diff} = P_{slave} - P_{master}$ (pressure difference between the two acquisitions). $\Delta_e = e_{slave} - e_{master}$ (vapor pressure difference between acquisitions). $k_2' = k_2 - (R_d/R_v)k_1 (\approx 23.4\ \mathrm{K/hPa})$

The PyAPS tool (Jolivet *et al.*, 2011) calculate a Zenith Total Delay (ZTD) (Mateus *et al.*, 2015) perform a numerical integration of refractivity along the vertical profile at each grid node of the meteorological model (ERA-Interim, ERA5 in modern PyAPS), unlike many empirical models that calculate the ZTD at a single point and then multiply it by a mapping function. The single-path LOS delay is defined as (Equation 2, Jolivet et at., 2011):

$$L_{LOS} = \frac{1}{\cos(\theta)}\int_{Z_0}^{H}(n-1)dz \tag{2}$$

Where: θ is the local incidence angle. The term 1/cos(θ) acts as the geometric mapping factor.

One way to address the presence of turbulent and vertically stratified components in signal detection has been the development of global atmospheric models (GAM), including global and regional operational and re-analysis weather models (e.g., NARR, ERA-Interim, MERRA-2, HRES) (Cao *et al.*, 2021), a variety of research has demonstrated the potential of using GAM-based predictive corrections to mitigate tropospheric InSAR delays (Jolivet *et al.*, 2011; Kinoshita, 2021; Ulma *et al.*, 2021; Kiriu *et al.*, 2022; Chen *et al.*, 2022; Sailellah and Fukushima, 2023; Zhang *et al.*, 2023; Dogru *et al.*, 2023), these predictive approaches have become routine for correcting tropospheric delays (Cao *et al.*, 2021).

To improve the accuracy of InSAR measurements, methods such as that of Jolivet *et al.* (2011), which corrects for spatial and temporal variations of tropospheric stratification, have been proposed. This method generates tropospheric delay maps synchronized with SAR acquisitions from the ERA-Interim weather model, the transition to ERA5 (the successor from ECMWF) is particularly critical for tropical regions due to significant improvements in how the model handles the complex moisture dynamics characteristic of those environments (Hersbach *et al.*, 2020). By validating it in interferograms without deformation, it was found that removing the atmospheric signal before phase unwrapping minimizes errors in regions with complex topography.

Albino *et al.* (2020) evaluated two methods to correct atmospheric errors: the first method applying phase elevation correlations and, the second method applying global weather models, also, evaluated the ability of time series to detect deformation anomalies. For which they used a fixed threshold and the use of a cumulative sum control chart, to represent accurate deformation values, applicable to any volcano in the world.

Kinoshita (2021) developed a neutral atmospheric delay correction model for InSAR, using total zenith delay (ZTD) and horizontal gradient data from Global Navigation Satellite Systems (GNSS). Whose usefulness of the correction model was evaluated in ALOS-2 interferograms over the Kanto Plain in Japan.

Ulma *et al.* (2021) used the Correction Online GACOS to correct the tropospheric delay model of persistent backscatters in 81 Sentinel-1A images for subsidence estimation in Surabaya, Indonesia, between 2017 and 2019.

Kiriu *et al.* (2022) evaluated the performance of three numerical weather models to mitigate tropospheric lag for InSAR applications in a tropical region. Their evaluation consisted of comparing the effectiveness of models to correct for atmospheric noise in Sentinel-1 interferograms at various spatial wavelengths. This analysis was performed using variograms to measure noise reduction, and GNSS data served as a benchmark against SAR-derived tropospheric delay estimates provided by the models.

For their part, Chen *et al.* (2022) researchers from Chengdu University of Technology-China proposed a method for topography-dependent atmospheric correction based on the multilayer perceptron (MLP) neural network model that combines spatial and topographic information data, in Sentinel-1 images, applied at the Baihetan Dam. The researchers contrasted the results with those obtained in the GACOS correction and the correction of the traditional linear model, where the MLP model reduced the phase standard deviation by 64%, being an indicator of the quality of the interferograms.

In turn, Sailellah and Fukushima (2023) researchers from Tohoku University compared the performance of two tropospheric delay correction methods for InSAR, in ALOS-2 data acquired over Japan. The first method consisted of the integration of the delay along the line of sight (LOS) of the mesoscale model (MSM) of the Japan Meteorological Agency (JMA) and; the second method employed GACOS correction that applies an iterative decomposition approach.

For their part, Zhang *et al.* (2023) performed multiple data simulations that included variable elastic deformation components. To solve the constraints problems on the weak flanks of the Common Scene Stacking (CSS) method under different deformation conditions, the researchers developed an iterative strategy. Their results indicated that the signal-to-noise ratio (SNR) is a key parameter affecting CSS performance in atmospheric phase display (APS) separation.

Dogru *et al.* (2020), seeking to overcome atmospheric effects in two of their InSAR studies, whose study areas were located in Central Anatolia between the period January 2016 and December 2018, and in East Anatolia between the period of September 2016 and December 2018 in Turkey, applied high-resolution ECMWF meteorological models together with an empirical phase elevation approach to correct the Sentinel-1 interferograms. Where the reduction of the standard deviation, being the indicative quality factor, worked better in the interferograms in descending mode for both studies.

In the present study, tropospheric correction was implemented using the PyAPS module. This tool, developed in Python 3, allows quantifying and correcting atmospheric noise of the type stratified in interferograms. The correction was made using ERA5 meteorological data on the area of interest in western Venezuela, corrected rates obtained with near 8 cm/y are more closely aligned with historical geodetic and topographic data recorded between 1926 and 1986, which showed approximately 5 meters of subsidence over 60 years. This suggests that earlier InSAR studies without correction may have produced less accurate or anomalous results due to unmitigated atmospheric interference. For the analysis, 157 Sentinel-1 interferograms were processed in the descending and ascending orbit directions, corresponding to the period 2018-2020 (Figure 1).

The ECMWF ERA5 model provides high-resolution atmospheric humidity, pressure and temperature data, essential for phase correction, of disturbances introduced by the atmosphere in the radar signal, in interferograms, for more accurate strain measurements (**https://www.ecmwf.int/en/forecasts/dataset/ecmwf-reanalysis-v5**). The ERA5 dataset provides information on the state of the global atmosphere, land and oceans. It allows the analysis of meteorological phenomena on a detailed scale, with a horizontal spatial resolution of $0.25° \times 0.25°$ for the atmosphere and $0.5° \times 0.5°$ for ocean waves, allowing the study of the evolution of the climate in the long term, with hourly estimates of a large number of atmospheric, terrestrial and oceanic variables, such as: temperature, humidity, wind, precipitation, solar radiation, etc.

Also, the model provides a deterministic correction for the stratified delay, the turbulent components are mitigated statistically through the inversion process, the linear trend estimation, and the selection of high-coherence pixels within the MintPy workflow (Yunjun *et al.*, 2019).

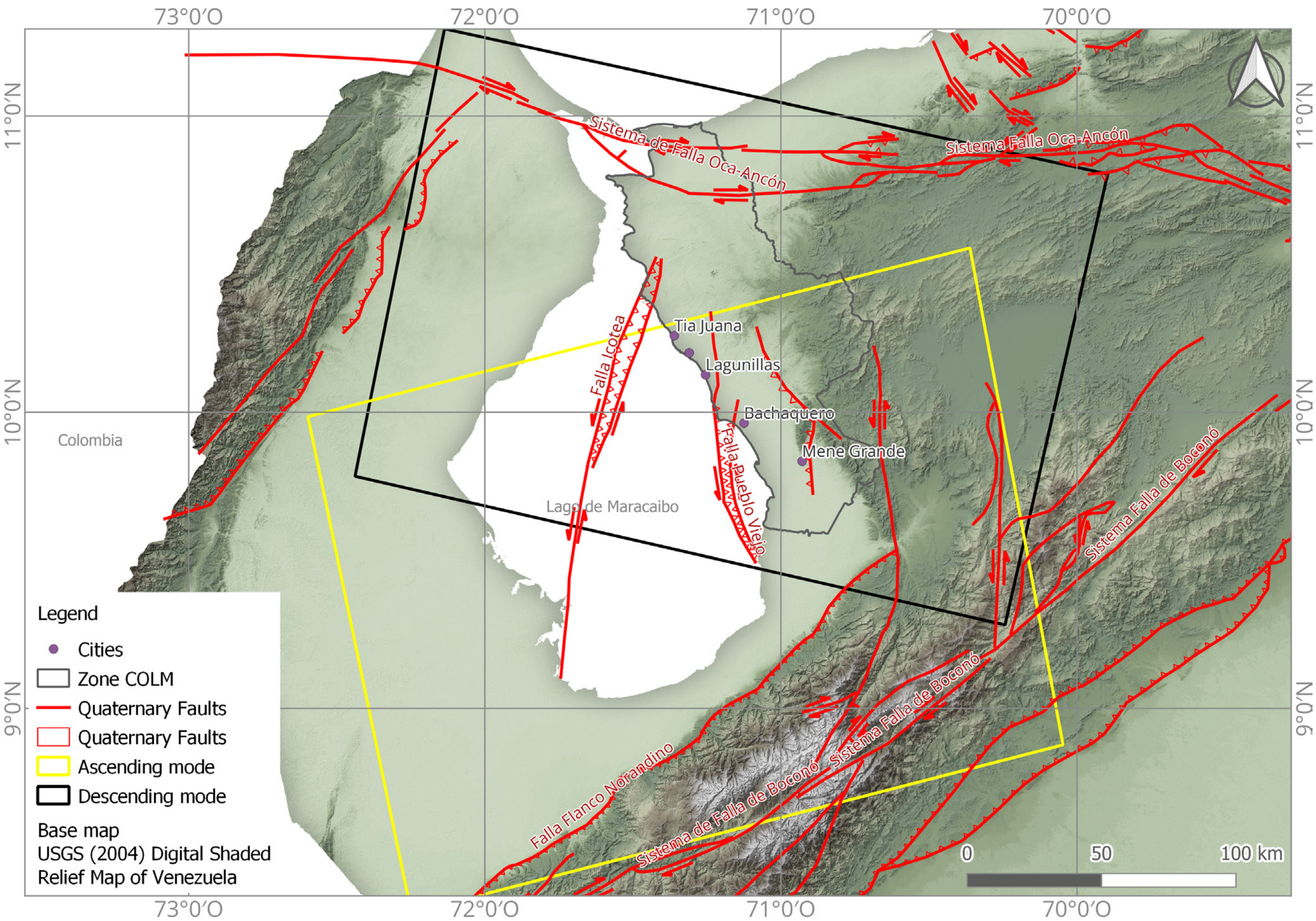

Figure 1. The frame of descending (black box) and ascending (yellow box) modes Sentinel 1 images. The area is surrounded by the fault systems of: Oca-Ancón (dextral strike-slip), Pueblo Viejo (reverse left-lateral strike-slip), Valera (left-lateral strike-slip), Icotea (reverse left-lateral strike-slip), Northern Foothills (thrust fault), Boconó (dextral strike-slip) (Audemard *et al.*, 2000).

2. Materials and Methods

The interferogram time series was generated using the ASF HyP3 (Alaska Satellite Facility's Hybrid Pluggable Processing Pipeline) platform (Hogenson *et al.*, 2020). For tropospheric correction, atmospheric data from the ERA5 model of the European Centre for Medium-Range Weather Forecasts (ECMWF), obtained through the Copernicus Climate Data Store (CDS), were used. These data were processed with the PyAPS based Atmospheric Phase Display estimation algorithm (Python), which generates differential phase delay maps caused by the stratified atmosphere to correct for radar interferograms (Yunjun *et al.*, 2019).

The selected scenes corresponded to the path/frame 171/557 in descending orbit and 4/25 in ascending orbit. For both modes, 78 pairs were generated for the descending mode and 79 pairs for the ascending mode, for the pair between January 2018 and December 2020. However, to ensure the quality of the interferograms, this study applied maximum recommended thresholds for the perpendicular baseline. The perpendicular baseline was limited to 100 meters to mitigate the topographic strips (see Figure 2), a criterion that only one interferogram exceeded. An small baseline is less distracted by the shape of the relief and can focus on the actual movement (displacement) of the soil. In COML region keeping the $B_{\perp}$ ensures the cms of movement are real ground displacements.

The temporal resolution was set at 12 days, determined by the availability of the images for both trajectory modes. Following this selection, 157 data pairs met all criteria. These selected pairs were processed on demand in HyP3 with the GAMMA software, obtaining products such as unwrapped phase (applying an threshold of 0.6 phase filter and water mask prior to time series inversion), wrapping phase, estimated coherence, etc. Subsequently, for tropospheric correction, it was processed with MintPy (Miami InSAR Time-series software in Python) (Yunjun *et al.*, 2019), this applies inversion algorithms of Subsets of Small Baselines (SBAS) (Berardino *et al.*, 2002) and uses the ERA5 model (Jolivet *et al.*, 2011) to perform the correction of tropospheric delay in time series using PyAPS.

3. Methodology

Tropospheric correction with PyAPS was implemented through MintPy (Yunjun *et al.*, 2019) by applying phase corrections directly to the time series, which is organized as a sequence of phases ordered chronologically with respect to a master acquisition. MintPy divides time series analysis into: interferogram network inversion for raw phase time series and, removal of tropospheric delay, topographic residue, timing error, and orbital error from the raw phase time series to derive the displacement time series (Yunjun *et al.*, 2019).

Instead of directly forming a set of interferograms with a single reference, the approach of inverting a reference interferogram network offers several advantages in analysis. It minimizes temporal decorrelation, phase information is preserved, and reduces the impact of spatial uncorrelation arising from topographic variations and geometric distortions, as well as reduces the impact of APS, which are source of error in InSAR analysis, where more accurate deformation measurements are obtained. In turn, the investment technique can handle missing data points, making it more robust to data breaches. Likewise, the least-squares calculation was employed to quantify the noise level within the time series. Also, the Weighted Least Squares (WSL) is used to manage connectivity and rank deficiency, only inverting the largest connected component and generanting a numInversion dataset for those pixels coherent in a few interferograms, masking out pixels that don't meet a minimum threshold of connectivity. According to the methodology developed by Yunjun *et al.* (2019) and implemented in Python, the step flow breaks down as follows (Figure 3).

The workflow described above was applied to the west region of Venezuela. As a result of InSAR processing, 157 interferograms were generated in their descending and ascending modes. Then, the velocity phase average maps from each dataset were generated in LOS view, shown in Figures 4 and 5 for the descending and ascending datasets.

The phase of each interferogram developed is relative to an arbitrary pixel. Therefore, the algorithm references all interferograms in a common reference pixel (in black color). The reference point step selects a common reference pixel for the interferogram stack. The default approach of Mintpy is to choose a pixel with the highest spatial coherence in the stack, in this case an threshold of 0.7 was used by default (Yunjun *et al.*, 2019).

Crustal deformation, caused by natural or anthropogenic processes, presents a linear behavior in a first approximation. To quantify it, the displacement rate is estimated, calculated as the slope of the linear fit of the time series. This calculation of the estimates the displacement velocity. Interpreting the resulting values, negative values indicate that the target is moving away from the radar (subsidence in vertical deformation). Positive values indicate that the target is moving towards the radar (uplift in vertical deformation).

The estimated velocity includes an expression of its uncertainty, which is derived directly from the goodness of linear fit. This uncertainty is quantified by the standard deviation of the residuals of the adjustment made to the time series.

However, the spatial pattern of the estimated standard deviation shows the spatial correlation of noise in the time series. The uncertainty depends on the distance, and increases with increasing pixel pitch. Figures 4b and 5b show each pixel's uncertainty relative to the reference pixel.

The intersection indicates the moment when the magnitude of the displacement and its variability (standard deviation) reach a point of significant relationship (Figures 4c,d and 5c,d). This point may indicate a change in the stability of the process that generates the displacements, which may coincide with an event that disturbed the stability of the displacements, such as a geological event, or a change in the activity that produces the

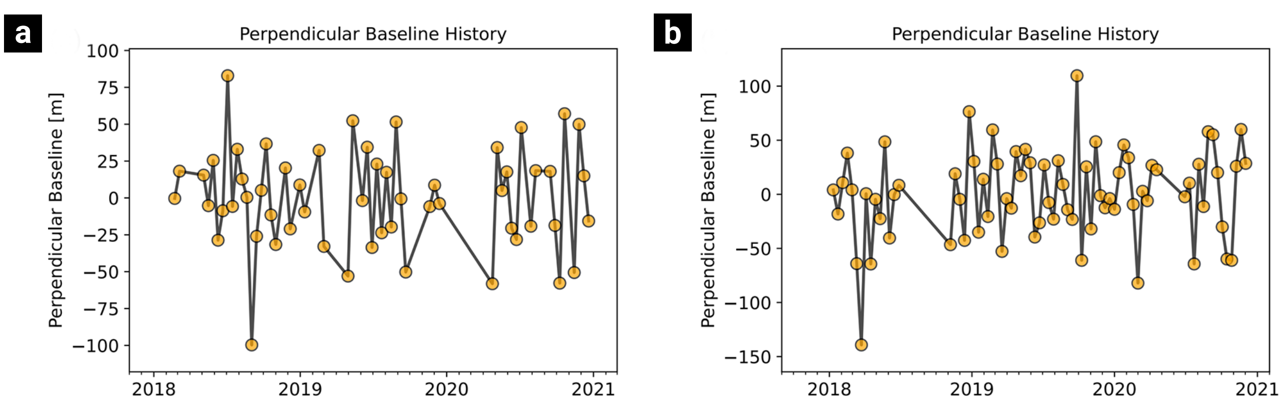

Figure 2. Baseline configuration for the 157 interferograms (a) ascending and (b) descending modes giving an overview of the network.

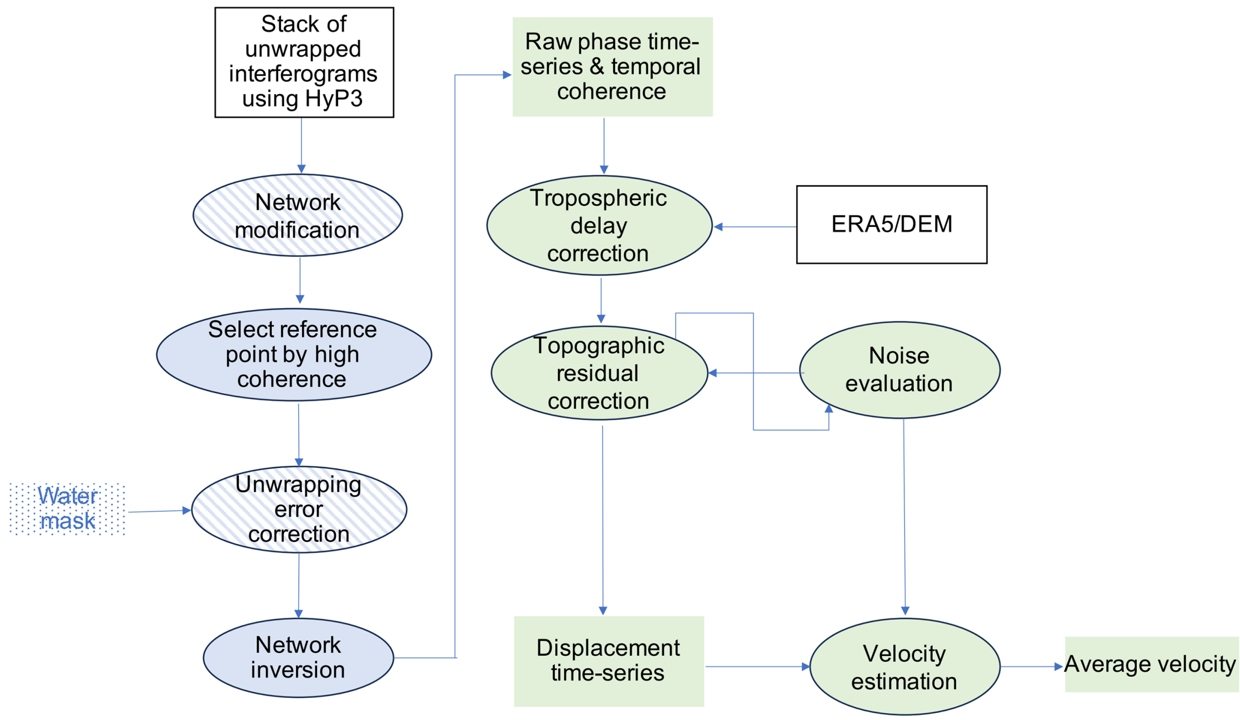

Figure 3. Flowchart adopted in this study (modified from Yunjun *et al.*, 2019).

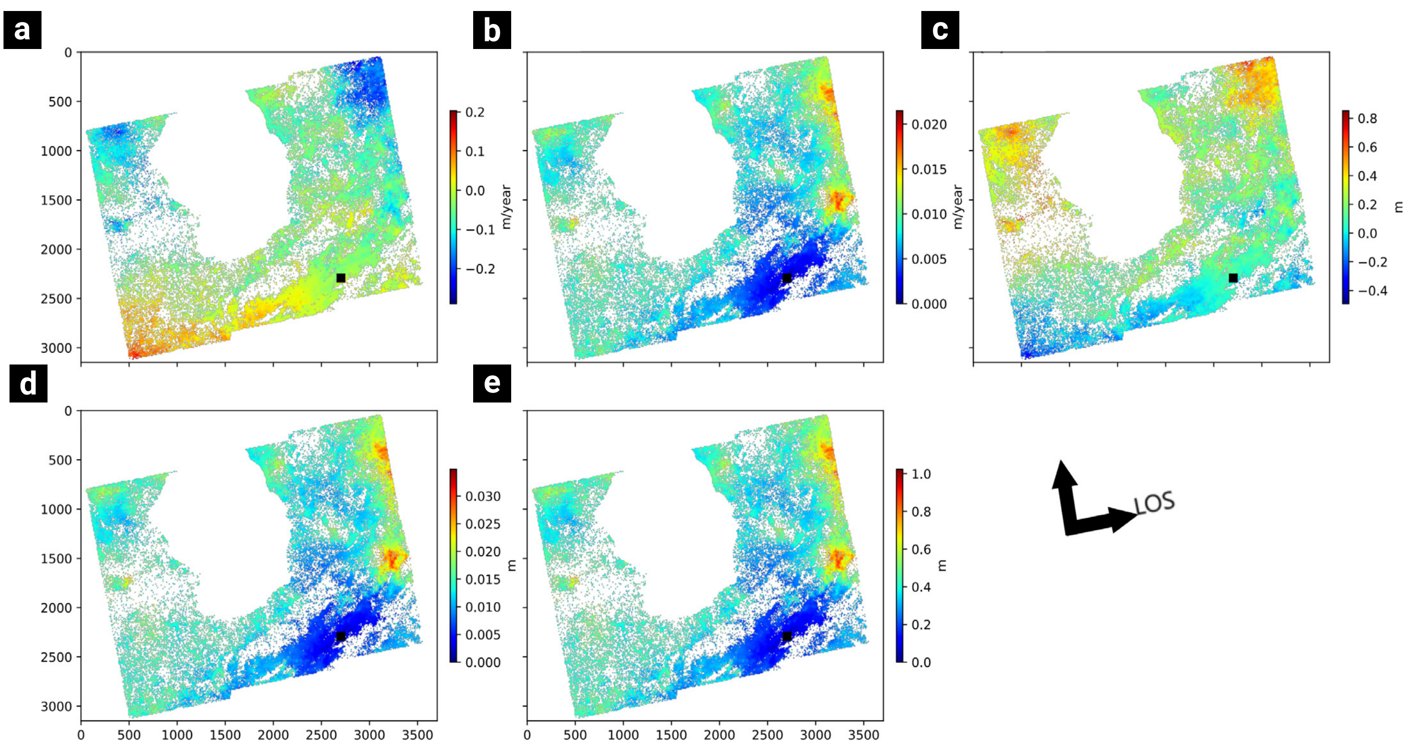

Figure 4. Annual displacement velocity for the period 2018-2019-2020 in LOS, in its ascending mode, for the west region of Venezuela (common reference pixel is given in black color)) (a) velocity, (b) standard deviation of velocity, (c) intercept, (d) intercept standard deviation, (e) residue.

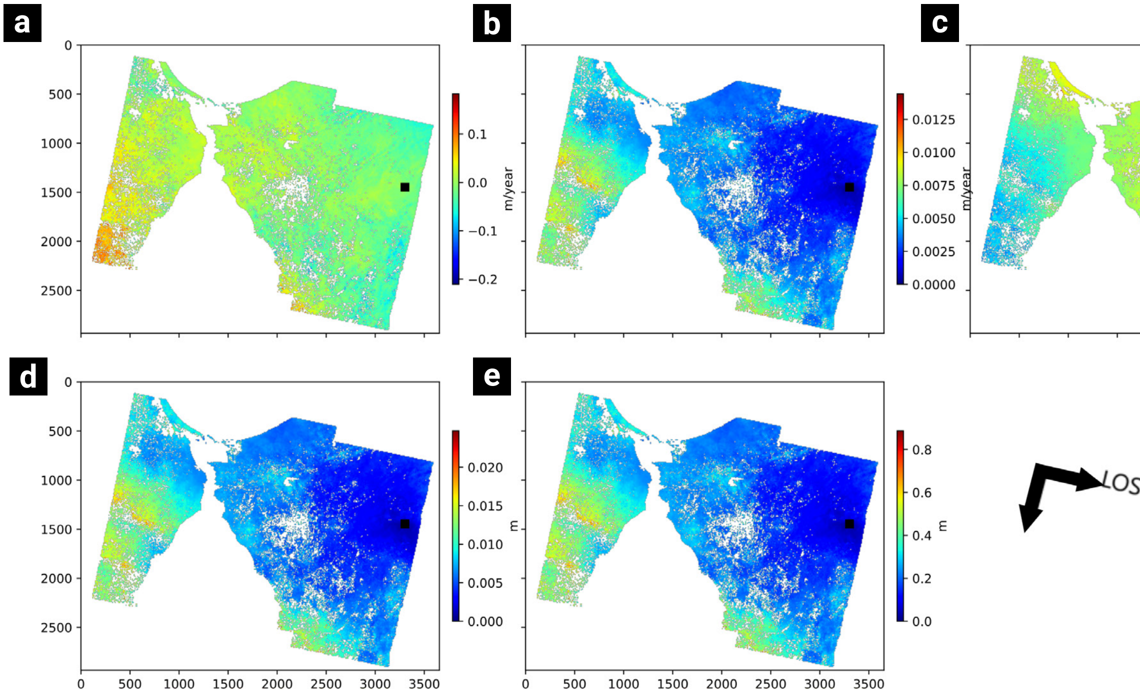

Figure 5. Annual displacement velocity for the period 2018-2019-2020 in LOS, in its descending mode, for the west region of Venezuela (common reference pixel is given in black color) (a) velocity, (b) standard deviation of velocity, (c) intercept, (d) intercept standard deviation, (e) residue.

displacements. The standard deviation quantifies the uncertainty associated with the intercept estimate. The residue provides the quality of the linear model fit, where small and random residuals indicate that the model is suitable (Figures 4e and 5e). Conversely, suppose the residuals show an increasing or decreasing trend, in that case, it suggests that the linear model may not be suitable for describing the deformation.

MintPy also calculates the temporal average of the spatial coherence of the entire stack as a possible auxiliary measure to choose reliable pixels after time series reversal, ranges from 0 to 1. Where pixels with values closer to 1 are considered reliable. For a dense network of interferograms, a threshold of 0.7 can be used (Yunjun *et al.*, 2019). The oil fields analized in COLM have stable infrastructure that maintain high coherence (> 0.8) regardless of the threshold. Therefore, the maximum subsidence rates reported (e.g., -7.9 cm/y) are likely very robust and insensitive to the threshold (see Figures 6 and 7).

4. Results and Discussion

The calculated phase delay is subtracted from the unwrapping interferogram to eliminate the effects of the atmosphere. It is a powerful and flexible tool for atmospheric correction of InSAR interferograms. Using high-quality data from the ERA5 model, PyAPS enables more accurate ground deformation measurements (see Figures 8 and 9), the atmospheric data are interpolated to the geometry of the InSAR image to obtain humidity, pressure, and temperature values at each image píxel.

The Maps of VelocityStd, represented like (b) in the figures 8 and 9, is referred to trust in the calculated speed of subsidence, represents the standard deviation of the linear fit residuals, low values < 0.5 cm/y, mean the ground is moving at a very steady, predictable rate. The atmospheric noise is low, and the linear model has a perfect fit for the data. High values > 1.5 cm/y, indicate that the scatter of the points around the line is high. This is usually caused by remaining turbulent atmospheric noise, soil moisture changes, or non linear ground movement (Yunjun *et al.*, 2019).

After of the PyAPS correction the values are between 0.1 cm/y and 0.6 cm/y (see Table 1) demonstrating excellent results, between excellent and an good adjustment of the model (see Table 2) with an high confidence in the displacement rates in LOS (see Figures 8 (b) and 9 (b)).

In previous InSAR investigations for the west region of Venezuela, specifically the East Coast of Maracaibo (known by their initials in spanish as COLM), surface deformation values have been obtained in the oil fields, with high agreement with linear historical rates (Murria & Saab, 1992) suggests that non linearities were not significant enough to change the overall

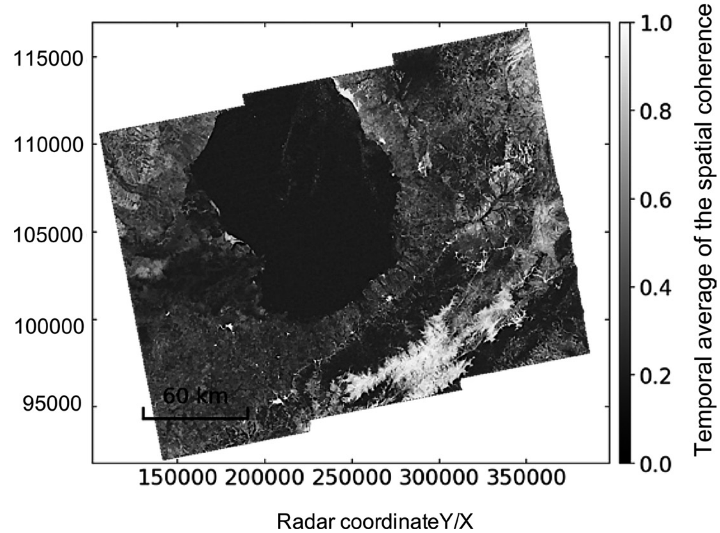

Figure 6. Average spatial coherence for the period 2018-2019-2020, in its ascending mode.

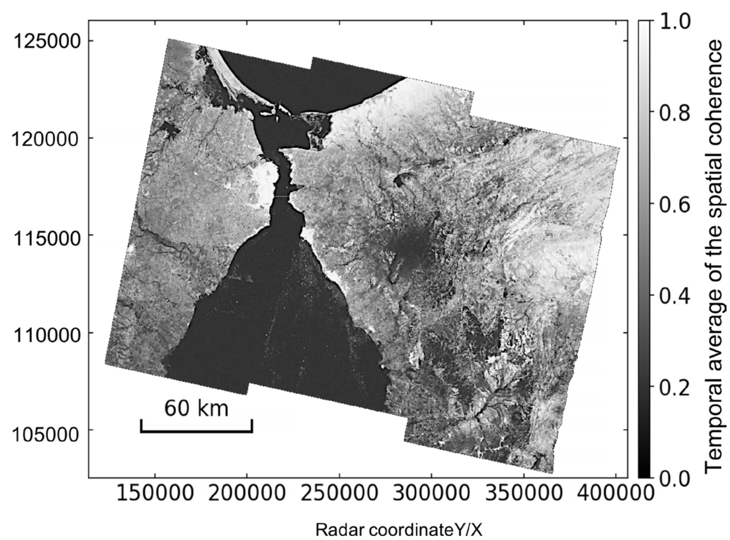

Figure 7. Average spatial coherence for the period 2018-2019-2020, in its descending mode.

interpretation of the subsidence hazard, annual velocity of displacement in LOS of the soil surface of -5.1 cm/y, -10.3 cm/y and -5.8 cm/y, respectively (Deguchi & Narita, 2015). Arenas *et al.* (2019) determined the subsidence of the COLM, using Sentinel 1 images, obtaining displacements between 2.8 cm/y and -2.8 cm/y in the areas of Cabimas, Tia Juana and Ciudad Ojeda for a period of three years. Quintana *et al.* (2021, 2025), applied the PSInSAR method for the ascending mode using 20 Sentinel-1 images, obtained displacement values in LOS ranging from -4.0 cm in the Lagunillas area, while in Ciudad Ojeda there is evidence of an uplift process of 4.5 cm/y, Tia Juana with 3.5 cm/y and Bachaquero with areas that rise towards the center of the city with 3.0 cm/y and areas that sink towards the NW with 2.0 cm/y. However, the application of atmospheric corrections in these studies was not mentioned, it can be inferred that the resulting values may be affected by atmospheric delays, causing them not to reflect the true velocity of displacements in LOS.

The estimated velocity values, obtained after the tropospheric PyAPS correction, specifically on the COLM, in LOS (in its ascending mode), for the surroundings of the Tia Juana, Lagunillas and Bachaquero fields respectively of -6.4 +/- 0.8 cm/y; -7.9 +/- 1.0 cm/y and; -7.1 +/- 0.8 cm/y (the uncertainty is refered to a temporal measure of the unmodeled noise) (see Figures 10 through 13).

The estimation of the annual displacement velocity values in LOS (in its descending mode) for the surroundings of the

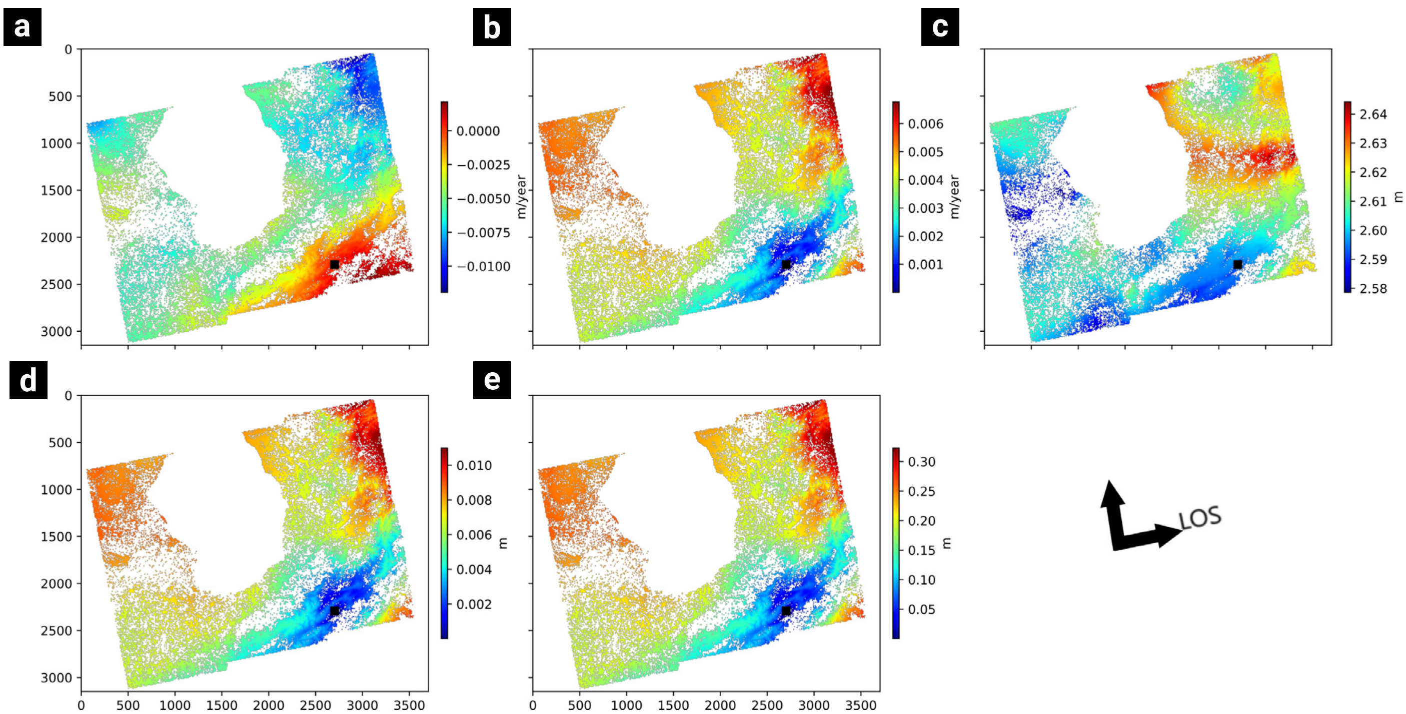

Figure 8. Displacement LOS rates after the calculated phase delay from the unwrapping interferogram for the period 2018-2019-2020 in LOS, in its ascending mode, correction based on the ECMWF ERA 5.

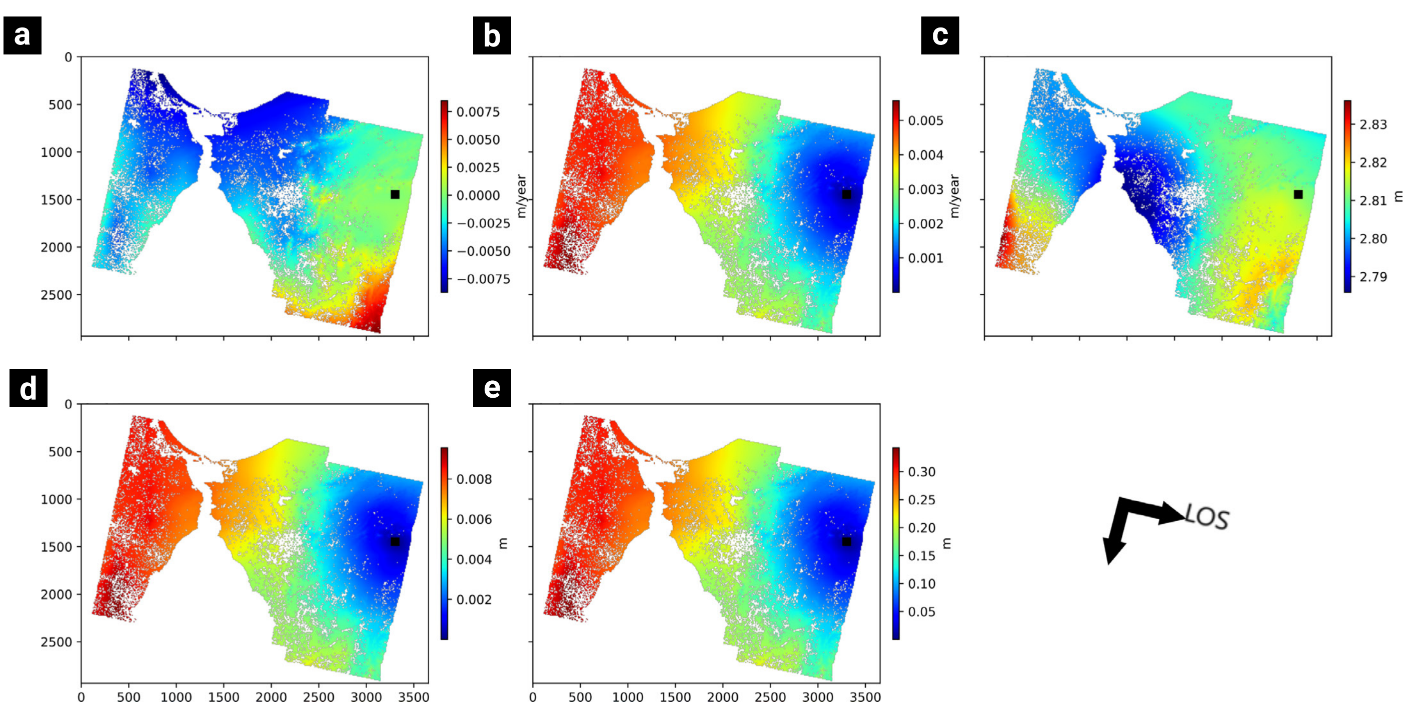

Figure 9. Displacement LOS rates after the calculated phase delay from the unwrapping interferogram for the period 2018-2019-2020 in LOS, in its descending mode, correction based on the ECMWF ERA5.

Table 1. Quantitative validation of the correction PyAPS ERA5 in COLM for the period 2018-2019-2020 based in the Maps of VelocityStd.

	Maps VelocityStd	
	Before	**After**
Ascending	2 cm/y	0.6 cm/y
Mode	1.5 cm/y	0.5 cm/y
	1 cm/y	0.4 cm/y
	0.5 cm/y	0.3 cm/y
		0.2 cm/y
		0.1 cm/y
Descending	1.25 cm/y	0.5 cm/y
Mode	1 cm/y	0.4 cm/y
	0.75 cm/y	0.3 cm/y
	0.5 cm/y	0.2 cm/y
	0.25 cm/y	0.1 cm/y

Table 2. Qualitative validation of the correction PyAPS ERA5 in COLM for the period 2018-2019-2020.

Value Range (cm/y)	Interpretation	Meaning for the COLM study
0.0 - 0.5	**Excellent**	High confidence in the subsidence rates. Minimal noise.
0.5 - 1.0	**Good**	Standard noise levels for tropical C-band InSAR.
> 1.0	**Moderate/Poor**	Areas likely affected by vegetation or high atmospheric turbulence.

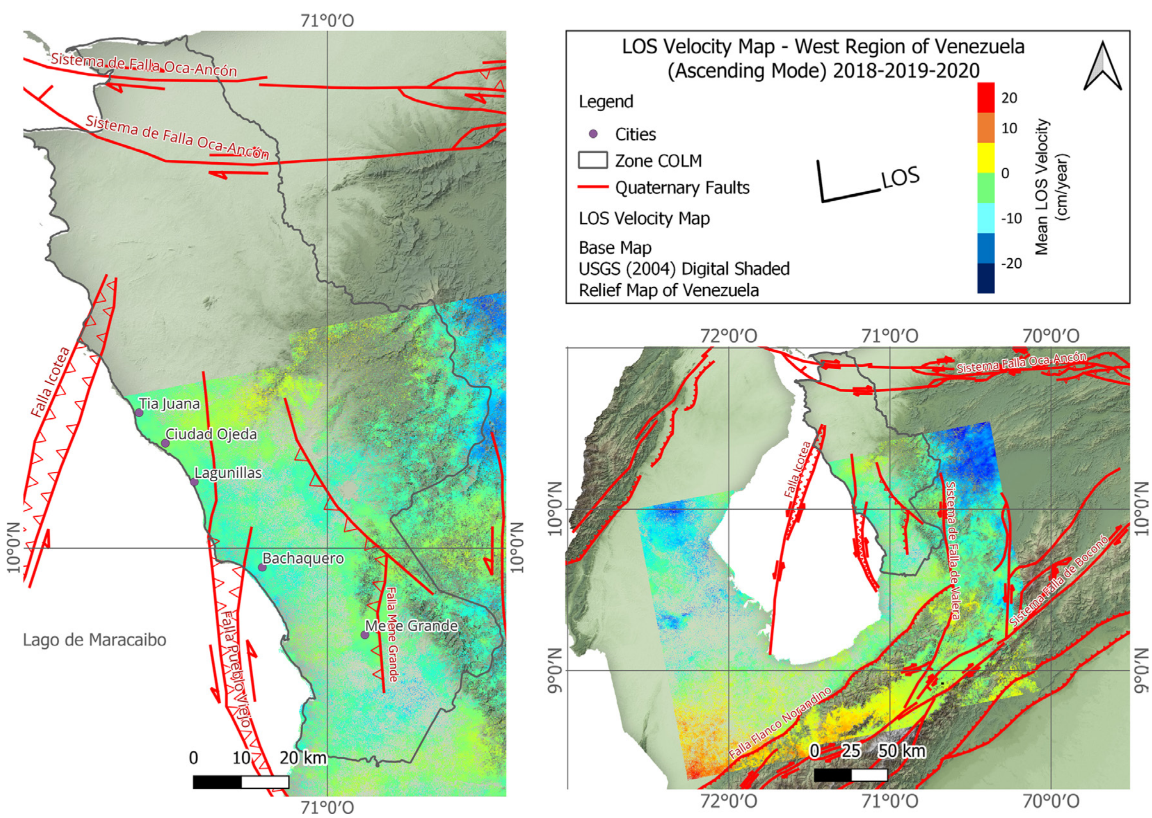

Figure 10. Annual values of displacement in LOS in the Tía Juana, Lagunillas, and Bachaquero oil fields, in ascending mode, for the period 2018-2019-2020.

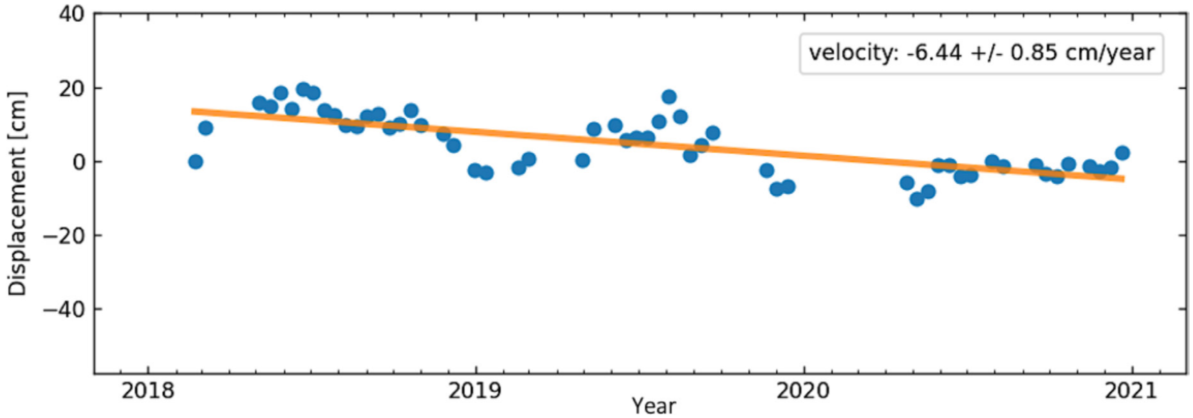

Figure 11. Displacement in LOS (cm/yr) for Tia Juana field, for the period 2018-2019-2020, in its ascending mode. The blue dots in the time series correspond to the cumulative offset values. In contrast, the orange line corresponds to the calculated trend line. The estimated values of the velocity and the uncertainties were calculated.

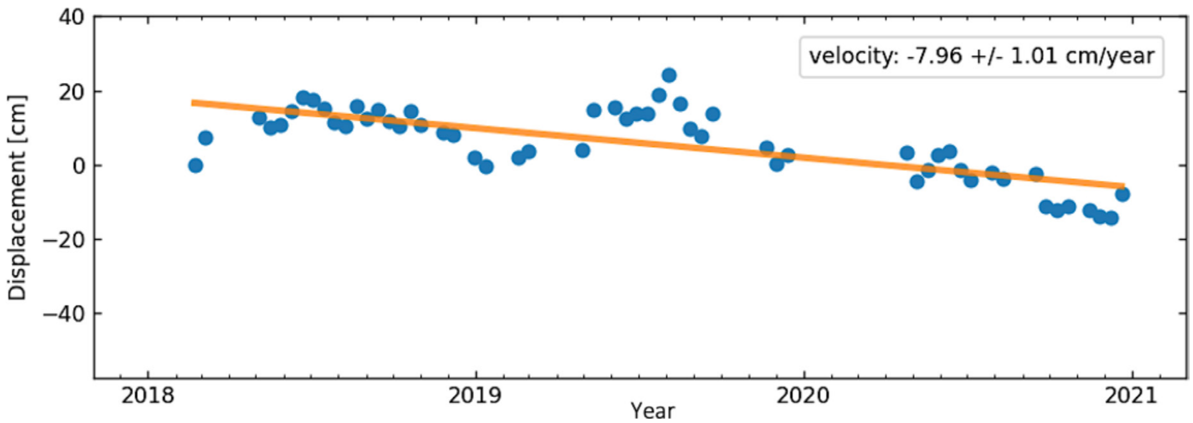

Figure 12. Displacement in LOS (cm/yr) for Lagunillas field, for the period 2018-2019-2020, in its ascending mode. The blue dots in the time series correspond to the cumulative offset values. In contrast, the orange line corresponds to the calculated trend line. The estimated values of the velocity and the uncertainties were calculated.

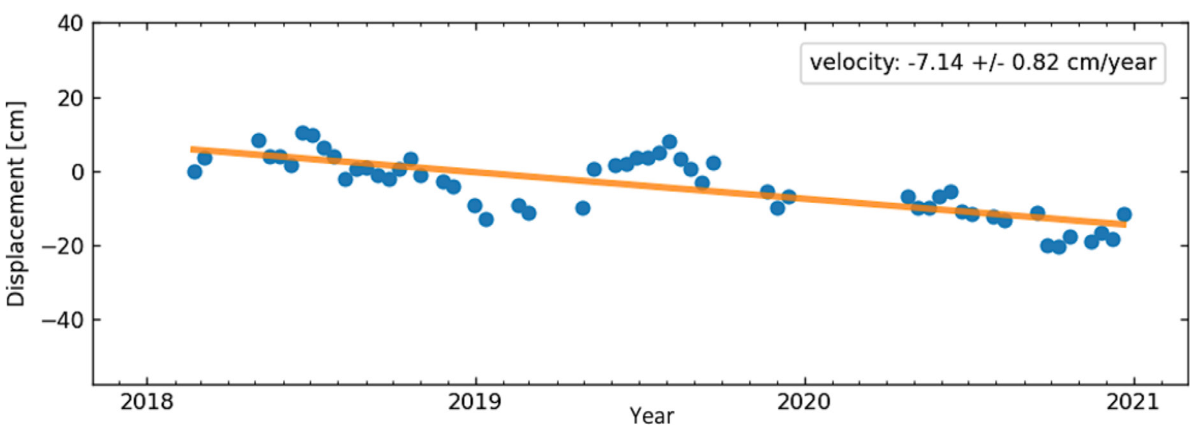

Figure 13. Displacement in LOS (cm/yr) for Bachaquero, for the period 2018-2019-2020, in its ascending mode. The blue dots in the time series correspond to the cumulative offset values, while the orange line corresponds to the calculated trend line. The estimated values of the velocity, and the uncertainties were calculated.

Tia Juana, Lagunillas and Bachaquero fields respectively of 1.2 +/- 0.5 cm/y; -4.1 +/- 0.5 cm/y and; -1.8 +/- 0.3 cm/y (the uncertainty is refered to a temporal measure of the unmodeled noise) (see Figures 14 through 17).

The different previous studies have applied different InSAR methods, DInSAR (Differential Interferometric Synthetic Aperture Radar) compares only two radar images from different dates. The topography, using a DEM, is subtracted to see what changed on the ground. PSInSAR (Persistent Scatterer InSAR) (Ferretti *et al.*, 2001) focuses on individual targets, such as infrastructures, that maintain high stability and signal backscatter over the entire study period; it connects every image to a single master reference, making it highly effective for monitoring urban infrastructure but less dense in rural areas and, and SBAS (Small Baseline Subset) (Hamzaoui *et al.*, 2025) included natural elements, by grouping images into multiple subsets with small spatial and temporal separations (baselines), minimizes the decorrelation and allows for a denser coverage of pixels in tropical terrains, like the areas surrounding the oil fields in the COLM region (see Table 3).

Also, it was possible to estimate delay tropospheric contribution and, the east-west and vertical components values using the Equation 3, combining the Standard Deviation (Std) and, ERA5 velocities in LOS in both modes, by decomposing the vectors, obtaining the contribution rates for the deformation, and dE and dU components to the three fields (see Table 4) (Equation 3, Fialko *et al.*, 2001, Hassen, 2001, Witkowski *et al.*, 2024).

$$U_e = \frac{dLOS_{desc}\, cos\theta_{asc} - dLOS_{asc}\, cos\theta_{desc}}{Denom}$$

$$U_u = \frac{dLOS_{asc}\,(-SIN\theta_{desc}\, SIN\alpha_{desc}) - dLOS_{desc}\,(-SIN\theta_{asc}\, SIN\alpha_{asc})}{Denom}$$

$$Denom = COS\theta_{asc}\, SIN\theta_{desc}\, SIN\alpha_{desc} - COS\theta_{desc}\, SIN\theta_{asc}\, SIN\alpha_{asc} \quad (3)$$

Where: $dLOS_{asc}$: displacement in LOS in its ascending mode; $dLOS_{desc}$: displacement in LOS in its descending mode; θ: Incident angle; α: Angle acimut.

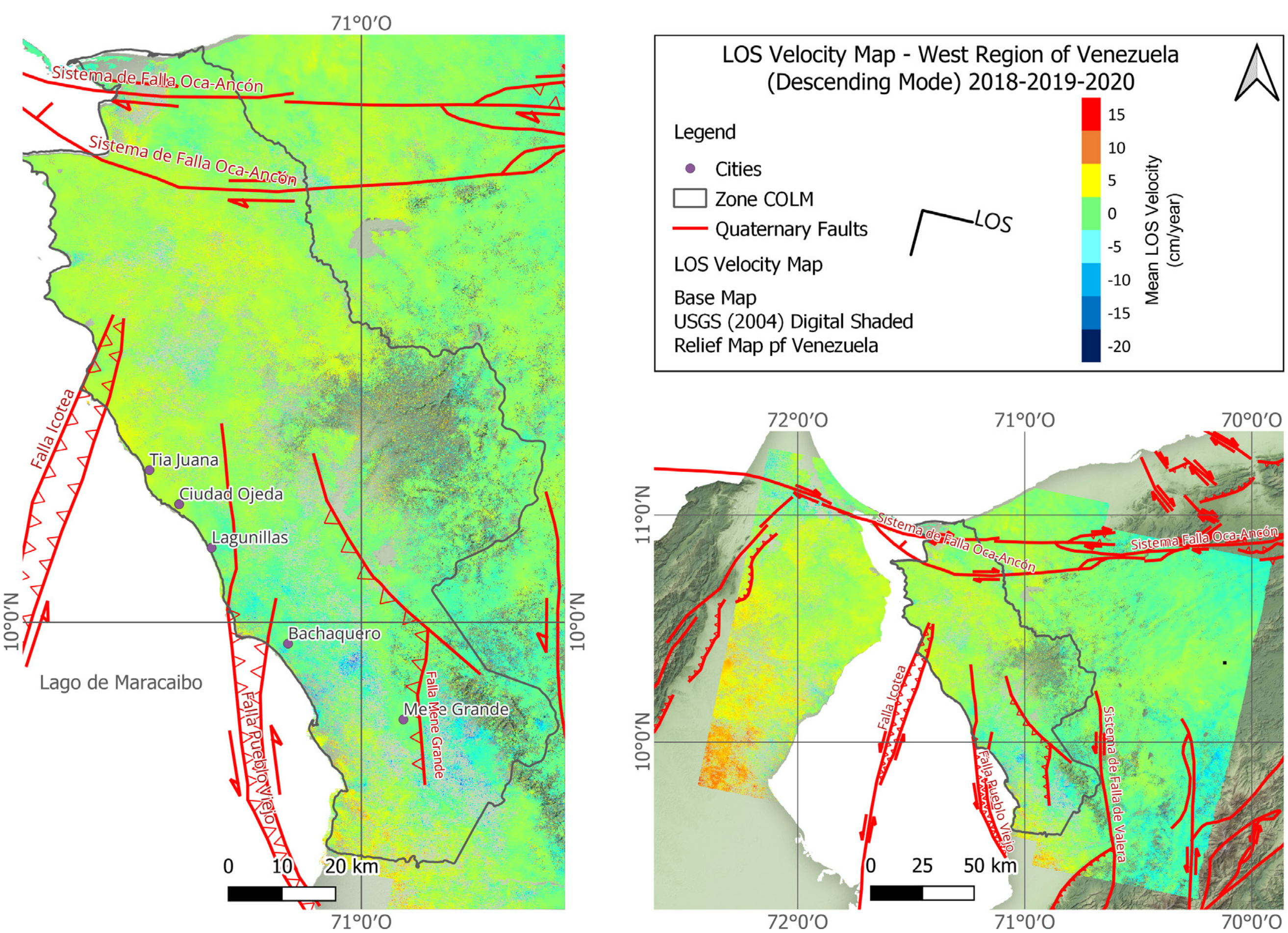

Figure 14. Annual values of displacement in LOS in the oil fields of Tía Juana, Lagunillas and Bachaquero, in descending mode, for the period 2018-2019-2020.

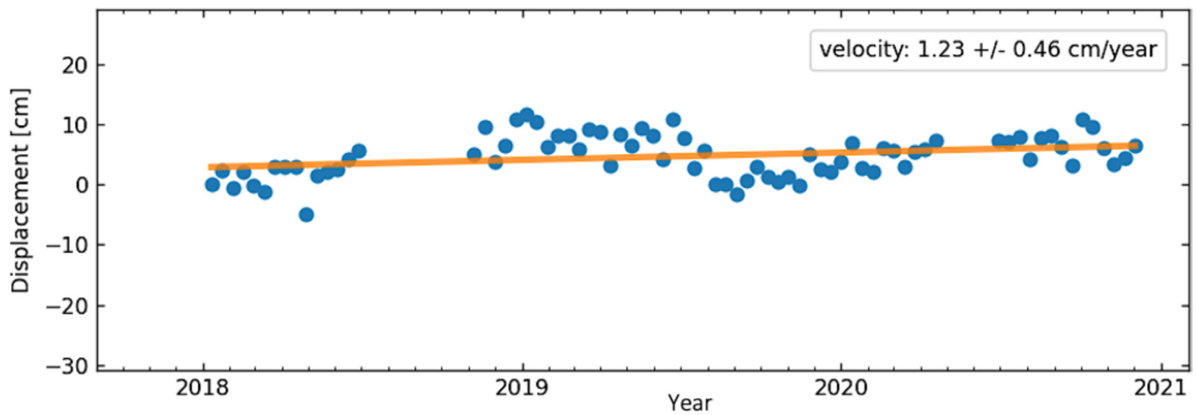

Figure 15. Displacement in LOS (cm/yr) for Tia Juana, for the period 2018-2019-2020, in its descending mode. The blue dots in the time series correspond to the cumulative offset values, while the orange line corresponds to the calculated trend line. The estimated values of the velocity, and the uncertainties were calculated.

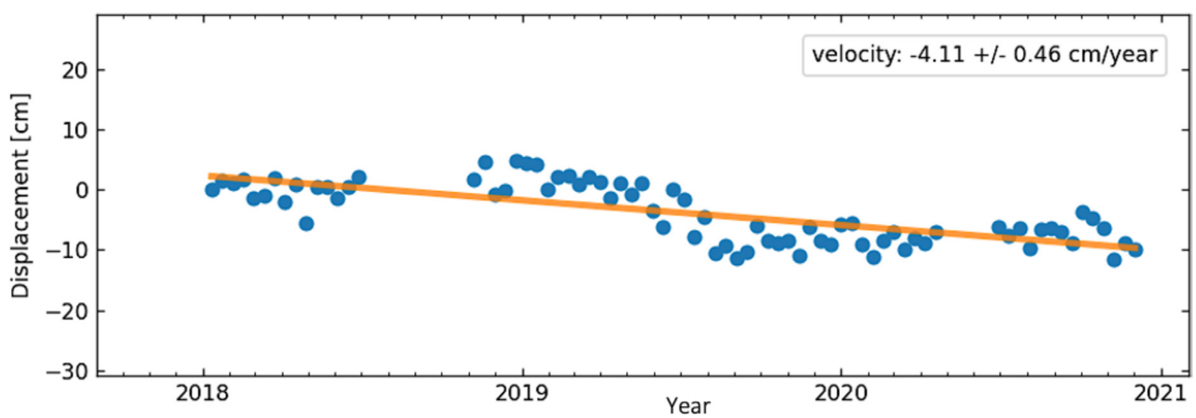

Figure 16. Displacement in LOS (cm/yr) for Lagunillas, for the period 2018-2019-2020, in its descending mode. The blue dots in the time series correspond to the cumulative offset values, while the orange line corresponds to the calculated trend line. The estimated values of the velocity, and the uncertainties were calculated.

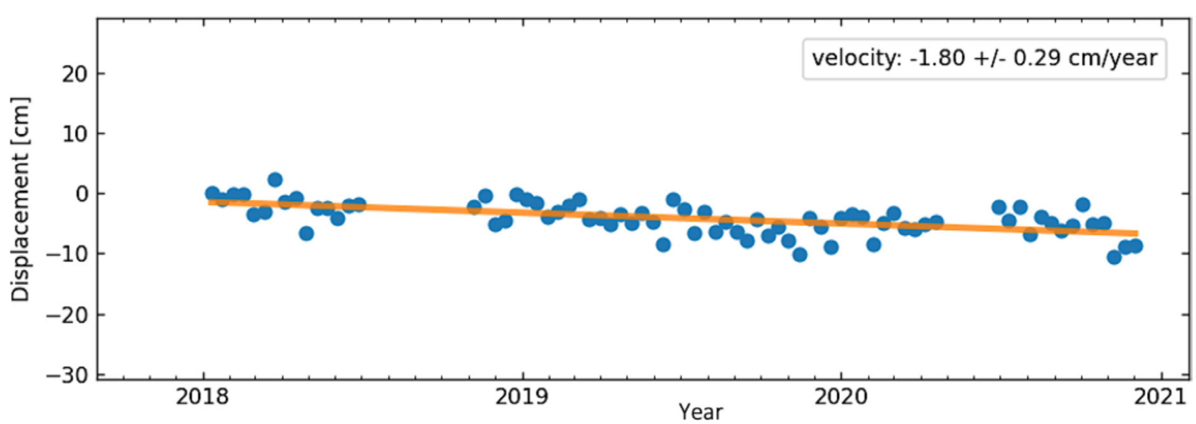

Figure 17. Displacement in LOS (cm/yr) for Bachaquero, for the period 2018-2019-2020, in its descending mode. The blue dots in the time series correspond to the cumulative offset values, while the orange line corresponds to the calculated trend line. The estimated values of the velocity, and the uncertainties were calculated.

Table 3. Comparative of values obtained in the COLM in the different studies conducted.

Zone	2021 (PSInSAR) Quintana *et al.*	2019 (DInSAR) Arenas *et al.*	2015 (DInSAR) Deguchi and Narita	2019 Arenas *et al.* (PCT 2006)
Lagunillas	- 4 cm		-10,3 cm	-3 cm
Ciudad Ojeda	4,5 cm	3 cm		5 cm
Tia Juana	3,5 cm	-3 cm	5,1 cm	-3 cm
Bachaquero	3 cm		-5,8 cm	-3 cm
	Quintana *et al.*, 2026 (SBAS)			
Zone	Displacement LOS in Ascending mode		Displacement LOS in Descending mode	
Tia Juana	-6.4 cm	+/- 0.8 cm	1.2 cm	+/- 0.5 cm
Lagunillas	-7.9 cm	+/- 0.1 cm	- 4.1 cm	+/- 0.5 cm
Bachaquero	-7.1 cm	+/- 0.8 cm	- 1,8 cm	+/- 0.3 cm

Table 4. Delay tropospheric contribution and, the East and Vertical components values using the Equation 3, combining the Standard Desviation (Std) and ERA5 velocities in LOS in both modes for Tia Juana, Lagunillas and Bachaquero oil fields to the period 2018-2019-2020.

Oil Fields	Delay tropospheric contribution dE (east-west) cm/y	Delay tropospheric contribution dU (up) cm/y	East-West and Vertical Components dE (east-west) cm/y	East-West and Vertical Components dU (up) cm/y
Tia Juana	-0.2	-0.6	-6.79	-2.94
Lagunillas	-0.3	-0.5	-3.27	-5.19
Bachaquero	-0.4	-0.5	-5.92	-6.29

The North-South displacement component was neglected due to the near-polar orbit of Sentinel 1, which results in low sensitivity to North-south motion.

Although the estimated tropospheric contribution (ranging from 0.2 cm/y to 0.6 cm/y) falls within the reported uncertainty margins of the deformation rates, its systematic nature poses a risk of cumulative bias in long term monitoring. By applying the PyAPS ERA5 correction, we effectively isolated the anthropic signal from topography dependent water vapor delays, ensuring that the calculated east west (dE) and vertical (dU) components reflect true reservoir compaction rather than atmospheric artifacts. This correction is particularly critical when contextualizing current rates against the 60 year historical subsidence of 5 meters, as it prevents the artificial inflation of deformation rates by approximately 5% to 8%, thereby providing a more rigorous baseline for ongoing dike stability and flood risk assessments in the COLM.

5. Conclusions

The InSAR technique is one of many applications of Remote Sensing suited for the COLM and Occidental Region of Venezuela studies, it solves the observational gaps inherent in traditional surveying, providing continuous monitoring, spatial density of data, and non invasive tool and cost effective for the monitoring of active oil fields without interrupting production or requiring ground access to potentially hazardous or restricted industrial zones. The methodology emphasized the atmospheric correction to tropical regions to obtain accurate values.

According to the obtained results, it is evident that the subsidence continues, specifically in the three oil fields of the COLM, with estimated LOS rates between -6 cm/y and -7 cm/y in its ascending mode and with values between -1 and -4 cm/y for Lagunillas and Bachaquero in its descending mode. However, Tia Juana presents positive values in descending mode. Also, for the estimation of the delay tropospheric contribution rates for the east and vertical components, the values between -0.2 to -0.6 cm/y and, the east-west (dE) and vertical (dU) components values for the three fields, with: -6.79 cm/y and -2.94 cm/y; -3.27 cm/y and -5.19 cm/y and; -5.92 cm/y and -6.29 cm/y respectively.

The study is further evidence of the importance of the application of atmospheric corrections when using the InSAR technique for the study of crustal deformations. When observing the values of the estimated tropospheric delay contribution, it is evident that the rates for the east and vertical components would be masked by atmospheric effects, affecting their accuracy. While the tropospheric signal might not be statistically significant in terms of overwhelming the error bars, it is geophysically significant. In a 3 years study (2018–2020), an uncorrected 0.6 cm/y atmospheric bias would result in a 1.2 cm error in total cumulative subsidence. For a region sensitive to millimetric changes in stability, this bias is too large to ignore.

Similarly, the InSAR technique is once again validated as suitable for the measurement of displacements, aimed at establishing the behavior of the subsidence phenomenon in a given period and also allowing the determination of its spatial distribution. However, since this technique is discrete in time, it is advisable to complement the measurements with continuous monitoring of geodetic data (e.g., cGPS/GNSS), by comparing InSAR displacement at GNSS station locations, ensuring that large scale atmospheric artifacts aren't interpreted as broad regional subsidence, validate the PyAPS/ERA5 correction, and to detect subtle, non linear deformation that would otherwise be buried under the phase grass of turbulent atmospheric noise.

It is recommended to continue the study with the extension of the temporality in the East Coast of Lake Maracaibo-COLM, and to correlate these results with the GNSS studies.

In conclusion, we can point out that the subsidence rates obtained by InSAR technique in the COLM, over a time window of 3 years (01/2018-12/2020), are very similar to the rates already obtained close to 8 cm/y, over the long term (5 m in 60 years, between 1926 and 1986), by conventional geodetic or topographic methods prior to the satellite era. However, satellite measurements do not require such a long time monitoring due to their high accuracy.

Finally, this study contributes to Environmental Geology and Geomechanics in several ways, showed how fluid extraction can become the primary driver of geomorphological change, outpacing natural geological processes in the basin. The displacement rates found (-7.9 cm/y in Lagunillas) can be used by reservoir engineers to calculate compaction coefficients and pore pressure changes within the Mioceno and Eoceno formations.

6. Acknowledge

This publication is derived from the academic activities carried out as part of the Doctoral Program in Engineering Sciences at the Central University of Venezuela. The authors express their sincere gratitude to the journal's editorial team for their excellent editing of this article. We also thank the anonymous reviewers for their valuable comments and suggestions, which significantly contributed to improving the quality of this work.

7. References

Agram, P. S., Jolivet, R., Riel, B., Lin, Y. N., Simons, M., Hetland, E., Doin, M.-P., & Lasserre, C. (2013). New radar interferometric time series analysis toolbox released. Eos, Transactions American Geophysical Union, 94(7), 69–70. https://doi.org/10.1002/2013EO070001

Albino, F., Biggs, J., Yu, C., & Li, Z. (2020). Automated methods for detecting volcanic deformation using Sentinel-1 InSAR time series illustrated by the 2017–2018 unrest at Agung, Indonesia. *Journal of Geophysical Research: Solid Earth,* 125(2), e2019JB017908. https://doi.org/10.1029/2019JB017908

Arenas, I., Hernández, B., Royero, G., Cioce, V., & Wildermann, E. (2019). Detection of subsidence due to the effect of oil extraction applying the DInSAR technique in Venezuela. *Revista Mapping,* 28(195), 18-26. https://ojs.revistamapping.com/MAPPING/article/view/204/67

Audemard, F. A., Machette, M. N., Cox, J. W., Dart, R. L., & Haller, K. M. (2000). *Map and database of Quaternary faults in Venezuela and offshore regions* (Open-File Report 2000-018). U.S. Geological Survey. https://doi.org/10.3133/ofr0018

Berardino, P., Fornaro, G., Lanari, R., & Sansosti, E. (2002). A new algorithm for surface deformation monitoring based on small baseline differential SAR interferograms. *IEEE Transactions on Geoscience and Remote Sensing,* 40(11), 2375–2383. https://doi.org/10.1109/TGRS.2002.803792

Biggs, J., & Wright, T. J. (2020). How satellite InSAR has grown from opportunistic science to routine monitoring over the last decade. *Nature Communications,* (11), 3863. https://doi.org/10.1038/s41467-020-17587-6

Brencher, G., Henderson, S. T., & Shean, D. E. (2025). Removing atmospheric noise from InSAR interferograms in mountainous regions with a convolutional neural network. *Computers & Geosciences,* 194, 105771. https://doi.org/10.1016/j.cageo.2024.105771

Cao, Y., Jónsson, S., & Li, Z. (2021). Advanced InSAR tropospheric corrections from global atmospheric models that incorporate spatial stochastic properties of the troposphere. *Journal of Geophysical Research: Solid Earth,* 126(5), e2020JB020952. https://doi.org/10.1029/2020JB020952

Chen, C., Dai, K., Tang, X., Cheng, J., Pirasteh, S., Wu, M., Shi, X., Zhou, H., & Li, Z. (2022). Removing InSAR topography-dependent atmospheric effect based on deep learning. *Remote Sensing,* 14(17), 4171. https://doi.org/10.3390/rs14174171

Chen, H., Shen, Y., Zhang, L., Liang, H., Feng, T., & Song, X. (2025). Mitigation of tropospheric turbulent delays in InSAR time series by incorporating a stochastic process. *ISPRS Journal of Photogrammetry and Remote Sensing,* 222, 186-203. https://doi.org/10.1016/j.isprsjprs.2025.02.028

Deguchi, T., & Narita, T. (2015). Monitoring of land deformation due to oil production by InSAR time series analysis using PALSAR data in Bolivarian Republic of Venezuela. In *Proceedings of FRINGE'15: Advances in SAR Interferometry and Sentinel-1 InSAR Workshop* (ESA

Publication SP-731). European Space Agency. https://doi.org/10.5270/Fringe2015

Doğru, F. (2020). The importance of atmospheric corrections on InSAR surveys over Turkey: Case study of tectonic deformation of Bodrum-Kos earthquake. *Pure and Applied Geophysics,* 177, 5761–5780. https://doi.org/10.1007/s00024-020-02606-w

Doğru, F., Albino, F., & Biggs, J. (2023). Weather model based atmospheric corrections of Sentinel-1 InSAR deformation data at Turkish volcanoes. *Geophysical Journal International,* 234(1), 280–296. https://doi.org/10.1093/gji/ggad070

European Centre for Medium-Range Weather Forecasts. (s.f.). *ECMWF Reanalysis v5*. https://www.ecmwf.int/en/forecasts/dataset/ecmwf-reanalysis-v5

Ferretti, A., Prati, C., & Rocca, F. (2001). Permanent Scatterers in SAR Interferometry. *IEEE Transactions on Geoscience and Remote Sensing,* 39(1), 8-20. https://doi.org/10.1109/36.898661

Fialko, Y., Simons, M., & Agnew, D. (2001). The complete (3-D) surface displacement field in the epicentral area of the 1999 MW7.1 Hector Mine Earthquake, California, from space geodetic observations. *Geophysical Research Letters,* 28(16), 3063–3066. https://doi.org/10.1029/2001GL013174

González, P. J. (2024). Interferometric Synthetic Aperture Radar (InSAR). En E. Chaussard, C. Jones, J. A. Jenn, A. Donnellan. (Eds.), *Remote sensing for characterization of geohazards and natural resources* (pp. 53-70). Springer. https://doi.org/10.1007/978-3-031-59306-2_3

Gray, A. L., Mattar, K. E., & Sofko, G. (2000). Influence of ionospheric electron density fluctuations on satellite radar interferometry. *Geophysical Research Letters,* 27(10), 1451–1454. https://doi.org/10.1029/2000GL000016

Hamzaoui, Y., Civera, M., Miano, A., Bonano, M., Fabbrocino, F., Prota, A., & Chiaia, B. (2025). Hierarchical Clustering and Small Baseline Subset Differential Interferometric Synthetic Aperture Radar (SBAS-DInSAR) for Remotely Sensed Building Identification and Risk Prioritisation. *Remote Sensing,* 17(1), 128. https://doi.org/10.3390/rs17010128

Hanssen, R. F. (2001). *Radar interferometry: Data interpretation and error analysis*. Springer. https://doi.org/10.1007/0-306-47633-9

Hersbach, H., Bell, B., Berrisford, P., Hirahara, S., Horányi, A., Muñoz-Sabater, J., Nicolas, J., Peubey, C., Radu, R., Schepers, D., Simmons, A., Soci, C., Abdalla, S., Abellan, X., Balsamo, G., Bechtold, P., Biavati, G., Bidlot, J., Bonavita, M., ... Thépaut, J.-N. (2020). The ERA5 global reanalysis. *Quarterly Journal of the Royal Meteorological Society,* 146(730), 1999–2049. https://doi.org/10.1002/qj.3803

Hogenson, K., Kristenson, H., Kennedy, J., Johnston, A., Rine, J., Logan, T., Zhu, J., Williams, F., Herrmann, J., Smale, J., & Meyer, F. (2020). *Hybrid Pluggable Processing Pipeline (HyP3): A cloud-native infrastructure for generic processing of SAR data* [Software]. Zenodo. https://doi.org/10.5281/zenodo.4646138

Hu, Z., & Mallorquí, J. J. (2019). An accurate method to correct atmospheric phase delay for InSAR with the ERA5 global atmospheric model. *Remote Sensing,* 11(17), 1969. https://doi.org/10.3390/rs11171969

Jolivet, R., Grandin, R., Lasserre, C., Doin, M. P., & Peltzer, G. (2011). Systematic InSAR tropospheric phase delay corrections from global meteorological reanalysis data. *Geophysical Research Letters,* 38(17), L17311. https://doi.org/10.1029/2011GL048757

Kinoshita, Y. (2022). Development of InSAR neutral atmospheric delay correction model by use of GNSS ZTD and its horizontal gradient. *IEEE Transactions on Geoscience and Remote Sensing,* 60, 1-14. https://doi.org/10.1109/TGRS.2022.3188988

Kirui, P., Riedel, B., & Gerke, M. (2022). Performance of numerical weather products for InSAR tropospheric correction: A case study of a tropical region. *ISPRS Annals of the Photogrammetry, Remote Sensing and Spatial Information Sciences,* V-3-2022, 115–122. https://doi.org/10.5194/isprs-annals-V-3-2022-115-2022

Mateus, P., Nico, G., & Catalão, J. (2015). Uncertainty assessment of the estimated atmospheric delay obtained by a numerical weather model (NMW). IEEE Transactions on Geoscience and Remote Sensing, 53(12), 6710–6717. https://doi.org/10.1109/TGRS.2015.2446758

Medici, C., Del Soldato, M., Fibbi, G., Bini, L., Confuorto, P., Mannori, G., Mucci, A., Pellegrineschi, V., Bianchini, S., Raspini, F., & Casagli, N. (2024). InSAR data for detection and modelling of overexploitation-induced subsidence: Application in the industrial area of Prato (Italy). *Scientific Reports,* 14, 17950. https://doi.org/10.1038/s41598-024-67725-z

Meng, L., Yan, C., Lv, S., Sun, H., Xue, S., Li, Q., Zhou, L., Edwing, D., Edwing, K., Geng, X., Wang, Y., & Yan, X-H. (2024). Synthetic aperture radar for geosciences. *Reviews of Geophysics,* 62(3), e2023RG000821. https://doi.org/10.1029/2023RG000821

Murria, J., & Saab, J. A. (1992). Problems and solutions in emergency planning for Western Venezuela oilfields. Paper presented at the Tenth World Conference on Earthquake Engineering, Madrid, Spain. https://www.iitk.ac.in/nicee/wcee/article/10_vol10_5917.pdf

Poland, J. F., & Davis, G. H. (1969). Land subsidence due to withdrawal of fluids. En *Reviews in Engineering Geology* (Vol. 2, pp. 187-269). The Geological Society of America. https://doi.org/10.1130/REG2-p187

Quintana, G. (2021). *Estudio de las deformación de la corteza derivadas de la geodinámica a partir de la interferometría SAR (Radar de Apertura Sintética): ejemplos de aplicación (Kumamoto-Japón, Valencia y Costa Oriental del Lago de Maracaibo-Venezuela)* [Tesis de maestría, Universidad Central de Venezuela].

Quintana-Sánchez, G., Audemard, F., Reinoza, C., Dogru, F., & Alvarado, L. (2025). Estudio de las deformaciones de la corteza derivadas de la geodinámica a partir de la Interferometría SAR (Synthetic Aperture Radar): Aplicación a la Costa Oriental del Lago de Maracaibo-Venezuela. *Revista Cartográfica,* (110). https://doi.org/10.35424/rcarto.i110.5874

Sailellah, S. N., & Fukushima, Y. (2023). Comparison of tropospheric delay correction methods for InSAR analysis using a mesoscale meteorological model: A case study from Japan. *Earth, Planets and Space,* 75, 18. https://doi.org/10.1186/s40623-023-01773-z

Ulma, T., Mutiara Anjasmara, A., & Hayati, N. (2021). Atmospheric phase delay correction of PS-InSAR to monitor land subsidence in Surabaya. *IOP Conference Series: Earth and Environmental Science,* 936, 012033. https://doi.org/10.1088/1755-1315/936/1/012033

Witkowski, W., Łucka, M., Guzy, A., Sudhaus, H., Barańska, A., & Hejmanowski, R. (2024). Impact of mining-induced seismicity on land subsidence occurrence. *Remote Sensing of Environment,* 301, 113934. https://doi.org/10.1016/j.rse.2023.113934

Xiao, R., Yu, C., Li, Z., & He, X. (2021). Statistical assessment metrics for InSAR atmospheric correction: Applications to generic atmospheric correction online service for InSAR (GACOS) in Eastern China. *International Journal of Applied Earth Observation and Geoinformation,* 96, 102289. https://doi.org/10.1016/j.jag.2020.102289

Yunjun, Z., Fattahi, H., & Amelung, F. (2019). Small baseline InSAR time series analysis: Unwrapping error correction and noise reduction. *Computers & Geosciences,* 133, 104331. https://doi.org/10.1016/j.cageo.2019.104331

Zhang, Z., Feng, W., Xu, X., & Samsonov, S. (2023). Performance of common scene stacking atmospheric correction on nonlinear InSAR deformation retrieval. *Remote Sensing,* 15(22), 5399. https://doi.org/10.3390/rs15225399